Comparison of Travelling Wave Array and Classical ICRH Launchers: Spectral and Absorption Characteristics on WEST

Lara Kassem Hijazi[1,*], *Julien* Hillairet[1], *Rémi* Dumont[1], *Vincent* Maquet[2], and *Riccardo* Ragona[3]

[1]CEA, IRFM, F-13108 Saint-Paul-lez-Durance, France
[2]Laboratory for Plasma Physics, LPP-ERM/KMS, 1000 Brussels, Belgium
[3]Technical University of Denmark, Department of Physics, 2800 Lyngby, Denmark

Abstract. Ion Cyclotron Resonance Heating (ICRH) plays a central role in plasma heating and current drive in tokamaks, making the optimization of antenna systems essential for maximizing performance. In this context, a comparative analysis of classical and Travelling Wave Array (TWA) launchers is carried out to assess potential improvements in absorption efficiency and spatial localization of deposited power. Simulations using the EVE code focus on Hydrogen minority heating in a Deuterium plasma under a magnetic field of 3.657 T in WEST. The results show that Hydrogen absorbs the most power for parallel wavenumbers $k_{\|\max}$ between 8 and 10 rad/m. Peak absorption occurs near the plasma core at 55.5 MHz with a poloidal phasing angle of 45° between rows. Moreover, changing the sign of the TWA's toroidal spectrum i.e., launching waves in the opposite toroidal direction has a small impact on power absorption by Hydrogen.

1 Introduction

ICRH is a key plasma heating method in fusion devices due to its ability to deliver localized heating without encountering density cutoffs, making it effective in high-density plasmas [1]. Traditionally, classical ICRH launchers operate at high voltage and power densities, but the TWA launcher has emerged as a promising alternative [2]. The TWA launchers have advantages that are particularly attractive for reactor relevant conditions like broadband operation, improved RF coupling, and reduced voltage operation. A high power, non-cooled TWA mock-up was successfully tested up to 2 MW in vacuum at the TITAN testbed at CEA-Cadarache [2], paving the way for future integration in tokamaks [3]. This work investigates the potential of applying the TWA concept to ICRH in WEST [4], focusing on optimizing its radiated spectrum and power absorption. Through parametric analysis using the EVE code, the evaluation of key plasma and launcher parameters, showing that the dominant $k_{\|\max}$ remains stable, an essential feature for consistent and efficient power absorption [5]. WEST is equipped with three classical ICRH launchers capable of delivering up to 3 MW for 30 s or 1 MW in steady-state operation per launcher, providing a relevant benchmark for comparison [6].

This paper is structured as follows: Section 2 states all the used parameters. Section 2.1 provides a brief overview of the simulation method used for ICRH. Section 3 discusses the characteristics of ICRH for the development of the TWA at WEST, including the power spectrum peak, optimal wavenumbers and the impact of different poloidal parameters. Section 4 compares the classical launcher with the TWA. Finally, concluding remarks are presented.

2 Scenario Description

In this study, the ICRH scheme simulated for the WEST tokamak is based on the D(H) minority ion heating method [7]. The plasma parameters were chosen to match experimental conditions relevant to the WEST tokamak, ensuring that the simulations are consistent with current and future operational scenarios. Specifically, these parameters were selected based on a WEST pulse scenario (WEST #59141), where ICRH launchers were located at R_{ant} = 3.01 m at 2cm from the Last Closed Flux Surface (LCFS) at mid-plane. This pulse is a lower single null, with a stable 700 kA plasma current and line averaged density of $\sim 6.02 \times 10^{19}$ m^{-3}, a representative of a suitable scenario for ICRH and assumes a total RF power of 3.8 MW coupled to the plasma. The electron density and temperature profiles used in the simulations are illustrated in Figure 1.

2.1 Simulation approaches

Accurate modelling of the TWA ICRH system on WEST requires capturing wave plasma interactions beyond the limits of ray tracing methods, which rely on the WKB approximation and may fail when the RF wavelength exceeds plasma gradient scales [8]. For this reason, full wave simulations are necessary. In this study, the multi-dimensional full wave code EVE [9] was used to solve Maxwell's equations for ion cyclotron waves in WEST. EVE uses a spectral variational approach to compute the electric field distribution and absorbed power profiles for

*Corresponding author: lara.kassemhijazi@cea.fr

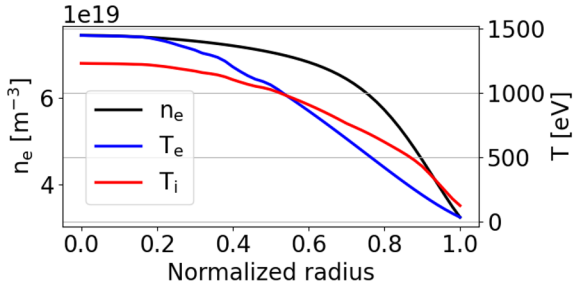

Figure 1. Temperature and density profiles for WEST #59141

ions and electrons, accounting for key absorption mechanisms such as ion cyclotron damping, mode conversion, electron Landau damping, and transit time magnetic pumping. Ion finite Larmor radius effects are included up to second order. To analyze the resulting fast ion distribution, EVE is coupled with the Fokker–Planck module AQL, which models anisotropic features of the ion distribution function [10].

For the absorption of waves, specifically in the case of Hydrogen ions as the minority species and Deuterium as the majority species, the Single Pass absorption rate (SPA) is calculated using the following analytical expression, derived from the single-pass wave absorption by H^+ minority fundamental resonance and D^+ majority second resonance heating [11]:

$$\mathrm{SPA} = 1 - e^{-2\eta}, \tag{1}$$

where

$$2\eta = \frac{\pi}{2}\frac{\omega_{pD}}{c}\frac{n_H}{n_D}\frac{Z_H}{Z_D}\frac{1}{1+\sigma^2} \tag{2}$$

and

$$\sigma^2 = \frac{\pi}{4}\left[\frac{n_H}{n_D}\frac{m_H}{m_D}\left(\frac{Z_H}{Z_D}\right)^2\right]^2\left(1-\frac{\omega_{c_D}^2}{\omega}\right)\left(\frac{\omega}{k_{\|0}v_{t_D}}\right)^2. \tag{3}$$

The subscripts D and H represent the Deuterium and Hydrogen ion species, ω_p is the plasma angular frequency, ω_c is the ion cyclotron angular frequency, ω the RF wave angular frequency, R the major radius, n the plasma density, m the ion mass, Z the ion's charge, $v_{t,i}$ the thermal velocity of the ion and c is the speed of light. The SPA is used to assess the ratio of Fast-Wave (FW) power absorbed by the plasma to the FW power entering the plasma. The SPA is not a direct output of the full-wave code EVE [9]. However, it can be approximated by dividing the total power absorbed by hydrogen by the total energy flux entering the plasma, mode by mode, according to the following expression inspired by Poynting's theorem:

In our formulation, the total absorbed power by Hydrogen (H) is given by:

$$P_{\mathrm{abs},H} = \int_V \frac{1}{2}\mathbf{E}^* \cdot \Im\left[\boldsymbol{\sigma}_H\right] \cdot \mathbf{E}\, dV, \tag{4}$$

Table 1. Partition of collisional power transfer (in %) for different TWA configurations.

Configuration	D (%)	e (%)
2x2	28.9	71.1
2x4	29.67	70.33
2x8	30.63	69.37

where $\boldsymbol{\sigma}_H$ is the complex conductivity derived from the cold plasma dielectric response. It should be noted that P_{abs} is integrated over the entire plasma volume.

The incoming electromagnetic power flux is computed as the surface integral of the time-averaged Poynting flux:

$$S_{\mathrm{Poynting}} = \int_{S_{\mathrm{plasma}}} \frac{1}{2\mu_0}\Re\left\{\mathbf{E}\times\mathbf{B}^*\right\}\cdot d\mathbf{S}, \tag{5}$$

where $d\mathbf{S} = \hat{\mathbf{n}}\, dS$ is the outward-oriented surface element evaluated at the plasma boundary ($\rho = 1$).

The Single Pass Absorption (SPA) is then defined as:

$$\mathrm{SPA} = \frac{P_{\mathrm{abs},H}}{S_{\mathrm{Poynting}}}. \tag{6}$$

This formulation follows the analytical approach described by Porkolab [11], and is consistent with global energy conservation as expressed by Poynting's theorem. It accounts for absorption by all species and avoids dependence on local quantities such as ρ or ψ.

3 Results and Analysis

3.1 Spectrum of TWA

Three TWA configurations with 2×2, 2×4, and 2×8 toroidal straps arranged in two poloidal rows were studied. As shown in Figure 2, increasing the number of toroidal straps narrows the radiated toroidal mode spectrum, thereby enhancing mode selectivity. This spectral narrowing reduces the excitation of parasitic coaxial modes, which are typically associated with higher impurity production. EVE simulations show that the partition of absorbed power among plasma species and the resulting collisional power transfer (Table 1) remain nearly unchanged for a given frequency and coupled power, as all configurations share a similar parallel wavenumber ($k_{\|}$). However, the absolute absorbed power density, as shown in Figure 3, increases with the 2×8 configuration, which exhibits both a narrower spectrum and reduced parasitic mode excitation. Consequently, the 2×8 TWA configuration was selected as the optimal trade-off between WEST's spatial constraints and the desired spectral and absorption characteristics.

3.2 Determination of the optimal toroidal mode number

Following the selection of the 2x8 configuration, it is essential to identify the optimum toroidal mode number n_{tor},

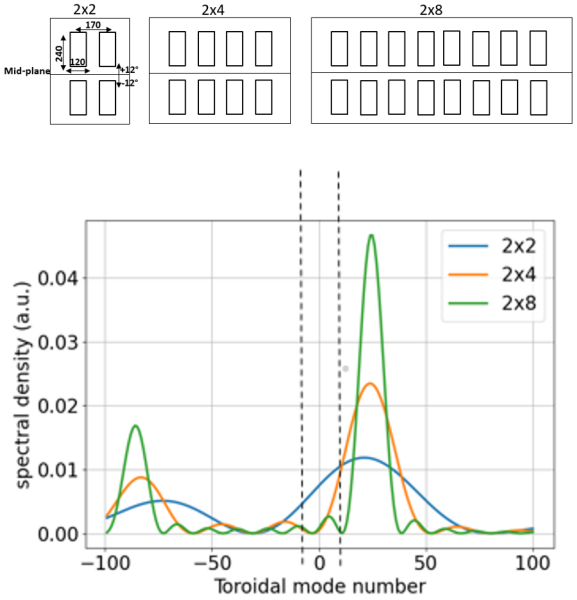

Figure 2. Top: TWA configurations (2×2, 2×4, 2×8; dimensions in mm). Each element is 120×240 mm with 170 mm inter-column spacing; the upper/lower rows are tilted by ±12° relative to the mid-plane; and toroidal phasing between straps around 80°. **Bottom:** Toroidal spectral density for the same total coupled power and frequency, corresponding to the layouts above, with vertical dashed lines indicate the toroidal mode numbers corresponding to the parasitic coaxial modes.

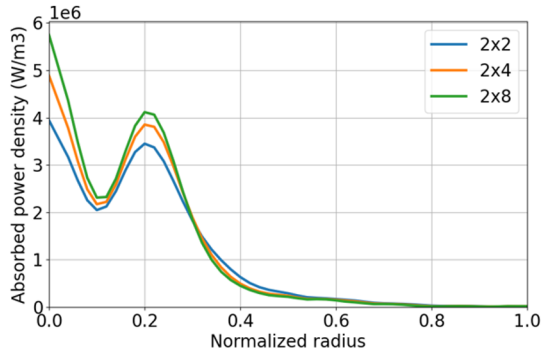

Figure 3. Absorbed power density by H for TWA configurations.

as its relation to the launcher geometry directly impacts the design. Figure 4 shows the ICRH single pass absorption for the WEST parameters, computed using equation (1). The plot illustrates how both the toroidal mode number and minority ion concentration affect SPA. Concentrations of 3% and 5% yield peak SPA values above 76%, occurring between $n_{\text{tor}} = 24$ and 40. Higher concentrations (8–10%) result in lower peak absorption, around 55–65%, within the same mode number range. SPA declines at mode numbers above 40, likely due to damping or scattering effects [12].

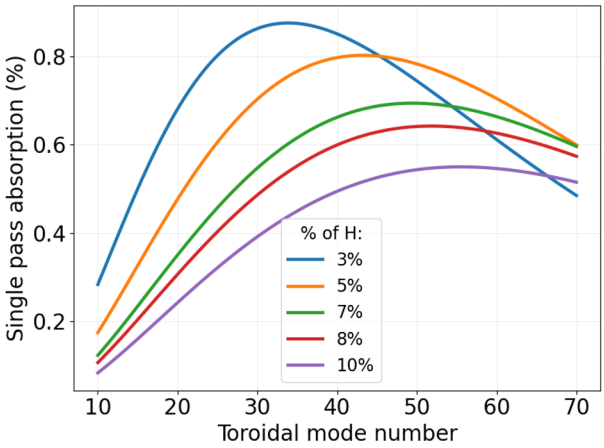

Figure 4. ICRF wave single-pass absorption for various Hydrogen concentrations, calculated using equation (1)

The results of SPA from EVE code are shown in Figure 5. The simulation reveals a maximum SPA reduction from 84% to 71% as % of H increases from 3% to 10%, while absorption decreases at lower ($n_{\text{tor}} < 24$) and higher ($n_{\text{tor}} > 40$) toroidal mode numbers due to resonance mismatch. Increasing the Hydrogen concentration reduces the SPA across the entire toroidal mode spectrum.

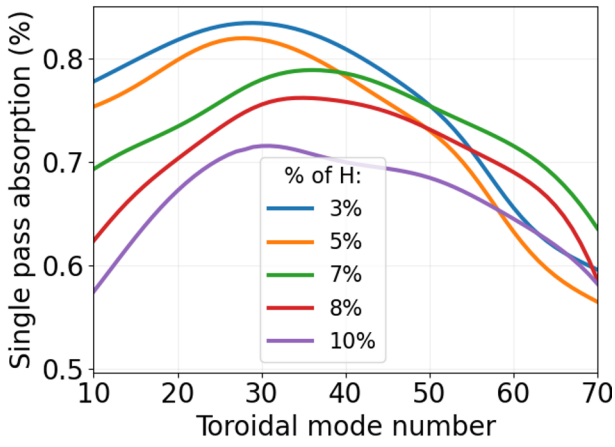

Figure 5. ICRH wave single-pass absorption at different Hydrogen concentrations, calculated using the EVE code.

The discrepancy between analytical and EVE results arises from the inclusion of the poloidal magnetic field in EVE, which is not described in the analytical model. At higher n_{tor}, the toroidal field dominates, leading to better agreement between both approaches. While both methods show reduced SPA with increasing H concentration, EVE also accounts for mode conversion, reflections, and multi pass effects.

Figure 6 shows the absorbed power among H, D, and electrons for a 5% H concentration, computed with EVE. Hydrogen absorption peaks below $n_{\text{tor}} = 70$, while electron absorption dominates at higher mode numbers due to increased $k_{\|}$, shorter parallel wavelengths, and phase ve-

localities resonant with electron thermal speeds. This enhances wave particle interactions via Landau damping. Consequently, mode numbers below 40 favor Hydrogen absorption at the fundamental cyclotron frequency, and $n_{\text{tor}} = 24$ is chosen for the upcoming simulations.

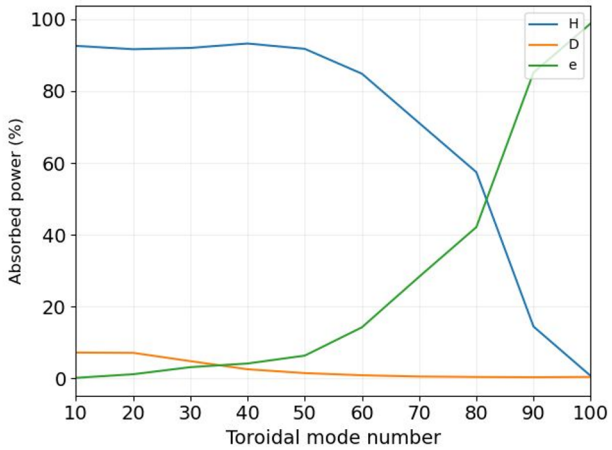

Figure 6. Partition of absorbed power between H, D, and electrons for 5% H concentration.

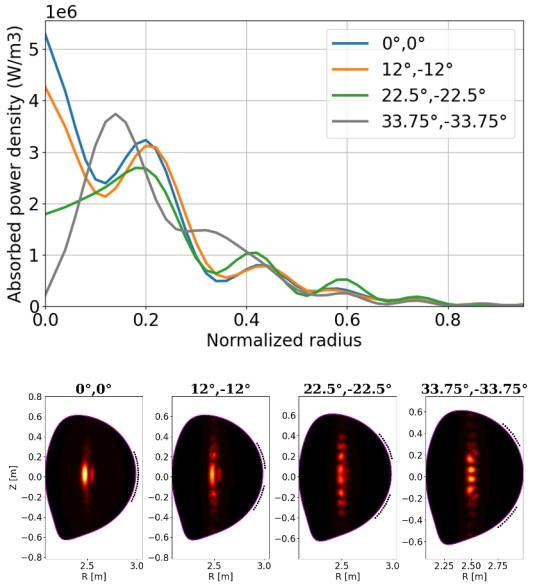

Figure 7. Comparison of absorbed power density by H. (a) 1D profiles versus normalized radius for various poloidal angle configurations. (b) 2D poloidal cross-sections showing absorbed power density; the curves near the low-field-side (LFS) edge indicate the poloidal positions of the upper and lower strap centers for each configuration.

3.3 Launcher's poloidal parameters

3.3.1 Poloidal angle between straps

The effect of changing the poloidal angle between straps on the power absorbed by H can be observed in 1D and 2D, where the latter refers to the angular displacement in the poloidal plane between the centers of the upper and lower strap rows, measured with respect to the machine midplane. In the 1D plot in Figure 7a, the absorbed power density reaches its highest peak at (0°,0°). As the poloidal angle between straps increases to larger values (±12°), the absorbed power density decreases. This continues as the position changes further to (±22.5°) and (±33.75°), where the absorbed power density remains lower than (0°,0°). The 2D plots 7b further illustrate this effect, showing how the spatial distribution of absorbed power density changes with poloidal position. At (0°,0°), the power is more focused along the central plasma region, while at higher poloidal angles, the absorption profile becomes more diffused and less intense. Due to mechanical integration constraints into WEST, the current preliminary design of the WEST TWA launchers has a poloidal position of ±12°.

3.3.2 Poloidal phase difference or poloidal launch angle

Increasing the poloidal phase difference between poloidal rows can increase the destructive interference of the fast magnetosonic wave near the equatorial plane, reducing on-axis heating performance [13]. WEST will include two rows of TWA launchers. As each row is fed by a dedicated high-power RF source, the phase between rows can be tuned by adjusting the phase between sources. The EVE code indicates that the poloidal phasing has minimal impact on the partition of the power absorbed by the different plasma species also on the collisional power transfer between D and electrons.

The results in Figure 8 indicate that a phase difference lower than 45° lead to a good absorbed power density, with a peak at a normalised radius of $\rho = 0$ at 55.5 MHz, while higher angles (e.g., 90° and 180°) result in significantly reduced power absorption density. This is attributed to changes in wave propagation, with increasing poloidal phase difference modifying the poloidal wave vector and wave interference effects, in particular destructive interference which weakens the effective wave amplitude, causing power to spread out and reducing power absorption density.

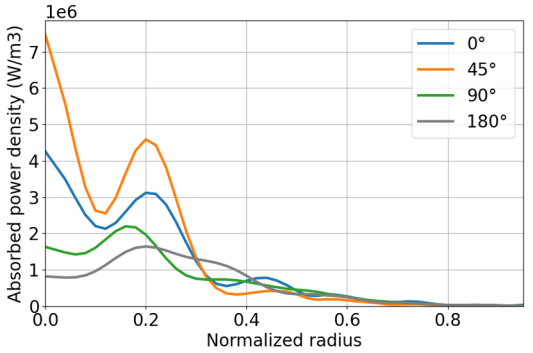

Figure 8. Absorbed power by H at different phasings for a poloidal position of ±12° in 1D.

The AQL module was used to evaluate the effect of poloidal phasing on the heated ion distribution function. Figure 9 compares the distributions for different phasing angles in both the perpendicular ($\lambda = 0$) and parallel ($\lambda = 1$) directions. At high energies, increasing the phasing angle significantly reduces the perpendicular distribution, with the 180° case showing the largest decrease in the high-energy tail. In contrast, the parallel distribution remains much less affected, with the curves for different phasings overlapping across most of the velocity range. This indicates that high phasing angles primarily impact perpendicular energy deposition, while parallel energy absorption stays relatively unchanged. Each distribution is calculated at the radial position where the absorbed RF power density reaches its maximum.

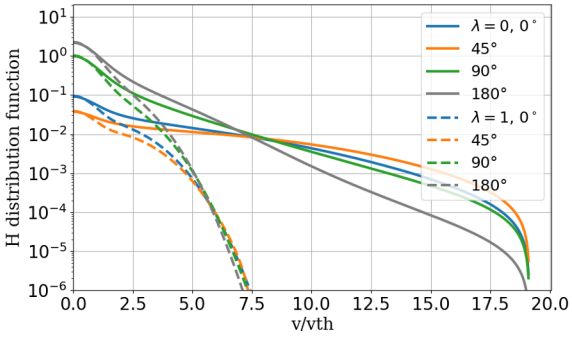

Figure 9. Comparison of the heated ion distribution function for different poloidal phasings at $\lambda = 0$ (perpendicular) and $\lambda = 1$ (parallel).

4 Comparison Between TWA and the Classical launcher at WEST

The TWA spectrum is compared with the one of the launchers presently installed at WEST by analysing power absorption in the plasma using the EVE code at the same power and frequency. The scenario examined involves minority heating D(H). The results indicate a notable difference between the two designs as shown in Figure 10. The spectral density analysis shows that the TWA launcher exhibits a sharp, dominant peak and a narrow spectrum, indicating strong mode selectivity. In contrast, the Classical launcher has a broader spectrum with two lobes, distributing power across several modes, which results in lower selectivity. This suggests that the TWA launcher is more effective in targeting specific modes and reducing unwanted spectral components.

Two different comparisons between TWA and the classical existing launcher at WEST are discussed. The first related to the effect of the % of H, where the absorbed power profiles indicate that the TWA launcher concentrates power deposition more effectively in the core region, particularly at low % of H (5% till 10%), whereas the classical launcher exhibits a broader but lower intensity absorption as shown in Figure 11. According to the

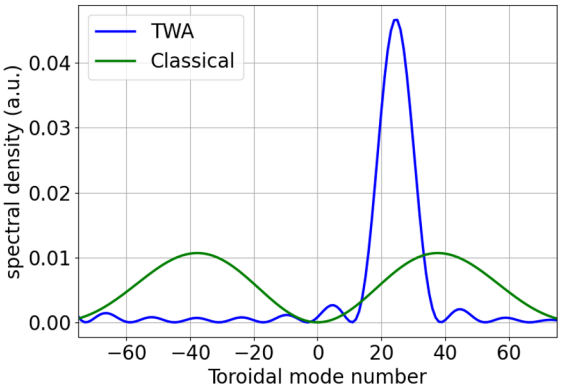

Figure 10. Toroidal spectra computed with the EVE full-wave code for the TWA (peaked at $n_c = 24$) and the conventional launcher (peaked at $n_c = 42$). The TWA exhibits higher directionality.

EVE code, the distribution of absorbed power between the plasma species, for both the TWA and classical cases, is roughly the same. Moreover, the small differences observed between both launchers in the collisional power partition in Table 2 indicate that the modifications introduced by the TWA to the Hydrogen distribution function have little impact on the overall energy redistribution between Deuterium and electrons. In both models, increasing the Hydrogen concentration leads to a clear shift in collisional power transfer from electrons to Deuterium, reflecting the stronger ion–ion collision as more power is absorbed by Hydrogen.

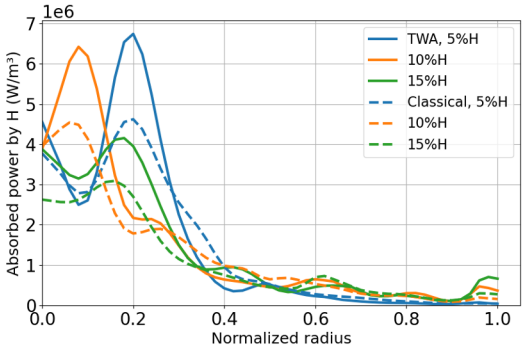

Figure 11. Absorbed power by H vs normalized radius at 55.5 MHz

Another comparison between TWA and classical launchers shows the influence of frequency on the absorbed power density by H in WEST. Figure 12a indicates that 54 MHz yields the highest power absorption density and strongest fast ion production, followed by 55.5 MHz, 52 MHz, and finally 62 MHz. The H distribution function supports this, showing a larger population of high-energy ions at 54 MHz. While greater absorption enhances heating, it also increases ripple induced fast ion losses in WEST. Thus, 54 MHz appears optimal, but a trade-off

Table 2. Partition of collisional power transfer (in %) for TWA and Classical launchers at different Hydrogen concentrations.

Configuration	D (%)	e (%)
TWA (5%H)	30.63	69.37
Classical (5%H)	31.44	68.56
TWA (10%H)	55.98	44.02
Classical (10%H)	55.17	44.83
TWA (15%H)	54.98	45.02
Classical (15%H)	54.93	45.07

between heating efficiency and confinement must be considered. This highlights how TWA's narrow spectrum enhances absorption by concentrating power in fewer modes.

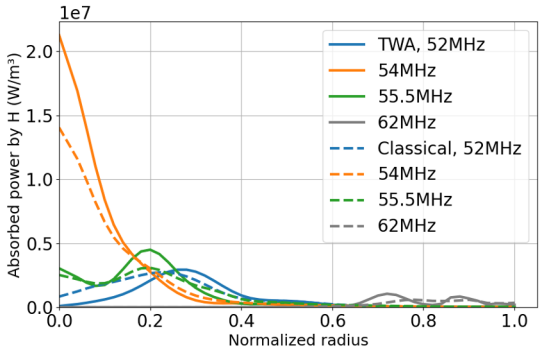

Figure 12. Comparison between TWA and classical launcher at different frequencies.

The performance of the TWA comes from its sharper and more selective power spectrum. Since both antennas operate at the same frequency, the resonance condition remains identical. However, the TWA concentrates power around a narrow range of $k_{\|}$, enhancing coupling to resonant ions and resulting in more localized core absorption and increased fast ion generation. In contrast, the broader spectrum of the Classical launcher spreads power over multiple $k_{\|}$ values, reducing absorption efficiency.

While we have previously assessed how the toroidal spectrum influences absorption, the effect of launching waves with negative toroidal mode numbers had not been explored. To address this, we study two additional cases: one where both poloidal rows emit with $n_c = -24$, and another case where one row emits with +24 and the other with −24.

Although EVE supports multiple toroidal modes in a single run, it cannot yet assign distinct n_c values to individual poloidal rows. Therefore, configurations combining $\pm n_c$ cannot be fully simulated. Importantly, summing results from separate $+n_c$ and $-n_c$ simulations is not equivalent to simulating both simultaneously, as the combined spectrum alters the poloidal structure.

In the simulations presented here, we compare TWA spectra centered at $n_c = +24$ and $n_c = -24$, corresponding to co- and counter-current launch. As shown in Figure 13, both yield similar absorption profiles for H, suggesting that minority heating is weakly sensitive to the sign of n.

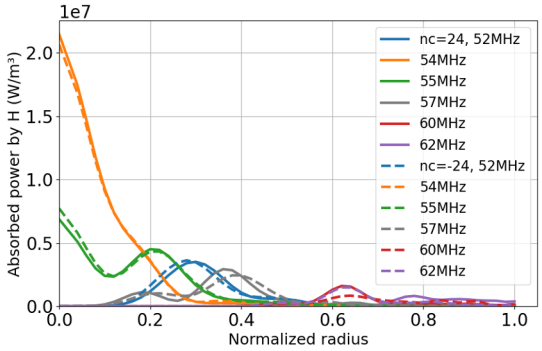

Figure 13. Absorbed power by H versus normalized radius.

5 Conclusion

D(H) minority ICRH scenarios for the WEST Tokamak were modelled using EVE code. The simulation results reveal that the ion cyclotron wave penetrates the WEST core plasma more effectively at $k_{\|max} = 8$ and 10 rad/m, where $k_{\|} = \frac{n_{\text{tor}}}{R_{\text{ant}}}$ with $R_{\text{ant}} = 3.01$ m.

A scan of various poloidal parameters reveal that the launcher's poloidal position, or the poloidal phasing between the two rows does not significantly affect the partitioning of the plasma species. After analysing different configurations for the launcher's poloidal position, it was found that poloidal launcher positioning and phase differences significantly influence wave propagation and absorbed power. Poloidal locations, such as 0° and ±12°, maximise wave absorption, with lower phase differences leading to more localised absorption near the core, while larger phase differences (90°, 180°) reduce absorption. Finally, the comparison between TWA spectra centered at $n_c = \pm 24$ has only a small effect on minority H absorption and the TWA launcher focuses power more in the core, while the classical launcher spreads it out but with less intensity.

Acknowledgments

This work has been carried out within the framework of the EUROfusion Consortium, funded by the European Union via the Euratom Research and Training Programme (Grant Agreement No 101052200 — EUROfusion). Views and opinions expressed are however those of the author(s) only and do not necessarily reflect those of the European Union or the European Commission. Neither the European Union nor the European Commission can be held responsible for them.

References

[1] M.J. Mantsinen, Experiments in high-performance jet plasmas in preparation of second harmonic ICRF heating of tritium in ITER, Nucl. Fusion **63**, 112015 (2023). https://doi.org/10.1088/1741-4326/aceb08

[2] R. Ragona, Status of the WEST travelling wave array antenna design and results from the high power mock-up, Nucl. Fusion **62**, 026046 (2022). https://doi.org/10.1088/1741-4326/ac4467

[3] R. Ragona, Travelling wave array antenna for efficient ICRH in fusion reactors, Plasma Phys. Control. Fusion **64**, 034002 (2023). https://doi.org/10.1063/5.0163430

[4] CEA-Cadarache, WEST tokamak, https://west.cea.fr (2024), accessed: 2024-11-19

[5] V. Maquet, R. Ragona, F. Durodié, J. Hillairet, Minimization of the edge modes and near fields of a travelling wave array antenna for WEST, arXiv preprint arXiv:2301.10754 (2023). https://arxiv.org/abs/2301.10754

[6] J. Hillairet, WEST actively cooled load resilient ion cyclotron resonance heating system results, Nuclear Fusion **61**, 096030 (2021). https://doi.org/10.1088/1741-4326/ac1759

[7] T.H. Stix, Waves in Plasmas (Springer Science & Business Media, 1992)

[8] B. Chaudhury, Comparison of wave propagation studies in plasmas using three-dimensional finite-difference time-domain and ray-tracing methods, Phys. Plasmas **13**, 1073 (2006). https://doi.org/10.1063/1.2397582

[9] R.J. Dumont, Variational approach to radiofrequency waves in magnetic fusion devices, Nucl. Fusion **49**, 075033 (2009). https://doi.org/10.1088/0029-5515/49/7/075033

[10] R.J. Dumont, D. Zarzoso, Heating and current drive by ion cyclotron waves in the activated phase of iter, Nucl. Fusion **53**, 013002 (2013). https://doi.org/10.1088/0029-5515/53/1/013002

[11] M. Porkolab, Plasma heating by fast magnetosonic waves in tokamaks, Thomas H. Stix Symposium p. 99 (1994). https://doi.org/10.1063/1.46754

[12] L. Chen, Z. Qiu, F. Zonca, Scattering by drift wave turbulence and damping of toroidal alfvén eigenmodes in burning plasmas, arXiv preprint (2022). https://doi.org/10.48550/arXiv.2204.09876

[13] P. Vallejos, Effect of poloidal phasing on ICRH power absorption, Nucl. Fusion **59**, 076034 (2019). https://doi.org/10.1088/1741-4326/ab1ab7